Optical extinction dependence on wavelength and size distribution of airborne dust

Garrett E. Pangle, D. Adam Hook, Brandon J. N. Long, C. Russell Philbrick, and Hans D. Hallen,
Physics Department, NC State University, Raleigh, NC 27695-8202

ABSTRACT

The optical scattering from laser beams propagating through atmospheric aerosols has been shown to be very useful in describing air pollution aerosol properties. This research explores and extends that capability to particulate matter. The optical properties of Arizona Road Dust (ARD) samples are measured in a chamber that simulates the particle dispersal of dust aerosols in the atmospheric environment. Visible, near infrared, and long wave infrared lasers are used. Optical scattering measurements show the expected dependence of laser wavelength and particle size on the extinction of laser beams. The extinction at long wavelengths demonstrates reduced scattering, but chemical absorption of dust species must be considered. The extinction and depolarization of laser wavelengths interacting with several size cuts of ARD are examined. The measurements include studies of different size distributions, and their evolution over time is recorded by an Aerodynamic Particle Sizer. We analyze the size-dependent extinction and depolarization of ARD. We present a method of predicting extinction for an arbitrary ARD size distribution. These studies provide new insights for understanding the optical propagation of laser beams through airborne particulate matter.

Keywords: aerosol scattering, optical extinction, non-spherical particles, Arizona Road Dust

1. INTRODUCTION

Optical extinction of light by dust particles dispersed in the air is an important problem. Dust storms are a dramatic example, and dusts are known to propagate for large distances in the atmosphere, and can impact optical transmission far from a desert. A better understanding of the optical properties of airborne particulate matter is important for future applications in optical communications, lidar measurements of atmospheric parameters and optical propagation through the atmosphere. The aerosols are also a climate-forcing agent, so knowledge of optical propagation through aerosols is required for accurate modeling of climate change. Better understanding of the scattering from particles allows an extension of Mie calculations to particulate matter [1]. A recent set of experiments examines the optical properties of Arizona Road Dust (ARD) disbursed into an atmospheric environment. The experiments investigate the effects of dust particle size on the scattering using sifted ARD to produce seven size cuts. Each size cut was studied at three different density distributions. An Aerodynamic Particle Sizer (APS) unit monitored the size distribution as a function of time while the larger, and then the smaller, particles settle out of the air. Studies of the combination of particle distributions cover a wide range of particle sizes. We use data from the size-selected samples to examine extinction due to small, medium, and larger particles in the ARD samples. The utility of this approach is tested by predicting the extinction from a distribution with a range of sizes and by combining data from three size-cut ranges, and comparing with simulations. Three laser wavelengths in the visible, the near infrared, and the long wave infrared (LWIR), are used to study the effects of the lofted dust on scattering and transmission. Each dust sample is injected into the test chamber to produce a cloud, which scatters the beams, and the two polarized components are measured in the forward and backward directions for each wavelength. The trials are of short time duration due to settling speed of the dust and a time sequence of measurements records the optical scattering as a function of the changing size distribution.

The polarization-dependent measurements enable an examination of the scattering contributions of irregular shaped particles and multiple scattering by ARD dust particles [2]. The polarized laser beams experience a measureable degree

Laser Radar Technology and Applications XVIII, edited by Monte D. Turner, Gary W. Kamerman,
Proc. of SPIE Vol. 8731, 87310N · © 2013 SPIE · CCC code: 0277-786X/13/$18 · doi: 10.1117/12.2017850

of depolarization when the scatters are non-spherical in nature, and when the density is high enough that multiple scattering occurs. The depolarization measurement is performed by comparing the cross-polarized signal with the signal in the laser polarization plane. The cross-polarized signal would remain at zero for the case of spherical aerosols under single-scattering conditions. Any significant variance from zero indicates a non-spherical particle and/or multiple scattering.

2. METHODS

2.1 Description of a measurement period

Prior to each trial during a set of experiments, a reference level for each detector is recorded for both polarization components in the forward and backward scatter directions of each beam. The relative detector efficiency is measured by rotating the plane of the laser beam by 90°. Comparing the measurements with the dust present to these reference levels provides the dust signature. The data are normalized by the reference levels to eliminate the need for full detector calibration and correction for the laser power, thus allowing a direct comparison of depolarization amplitude at each wavelength.

The dust sample is injected into the chamber while fans within the chamber loft and spin the dusty air, thereby simulating the wind suspension of atmospheric dust aerosols. The detectors record throughout the duration of each test, typically 10-15 min, while measuring the transmission loss and depolarization due to scattering by the dust. An Aerodynamic Particle Sizer (APS) records the concentration of the dust over time.

The size cuts of ARD are divided into seven samples and measurements are made at three concentration densities by injection of 20, 100, and 200 grams of dust into a volume of about 80 m^3 at the start of each trial run. Distinct samples of ARD are used for each trial; these include overlapping levels of 0-3, 5–10, and 10-20 microns, non-overlapping levels of 0-5, 0-10, and 0-20 microns, and the Ultrafine size (<15 μm sold by Powder Technologies, Inc.). Each of the distinct levels provides a portion of the particle size distributions selected for our investigation. Figure 1 shows the APS measurements of size distributions for the size cuts of 0-3, 0-5, 5-10, and 10-20 μm samples near the density peak occurring about 60 s just after the 100 gram injection. Each of the 100 gm tests shows that a fraction of the particles are less than 4 μm in diameter. That scattering is small compared to the signal produced by the particles at larger sizes, since the scattering cross section of the small particles is much less. At later times in a trial, the larger particles fall out of the distribution of aerosols, and scattering from the smaller particles still present becomes dominant.

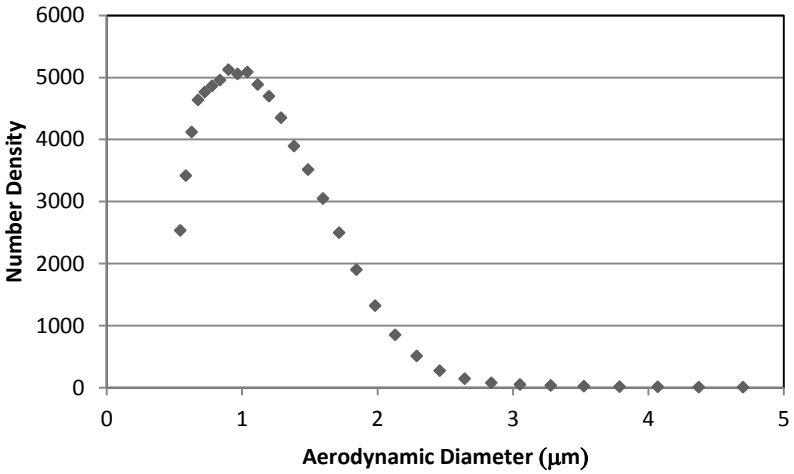

(a)

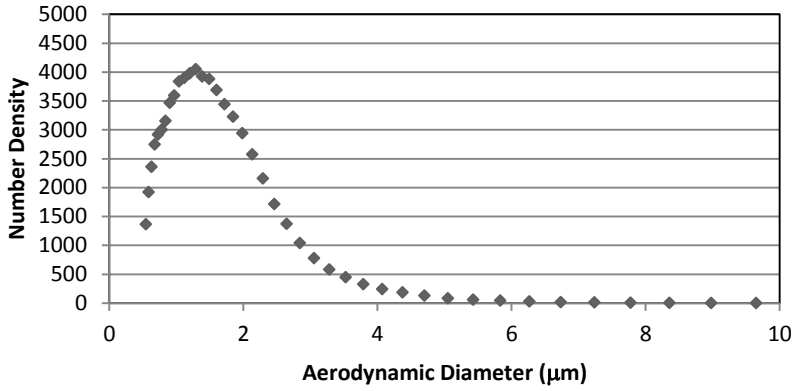

(b)

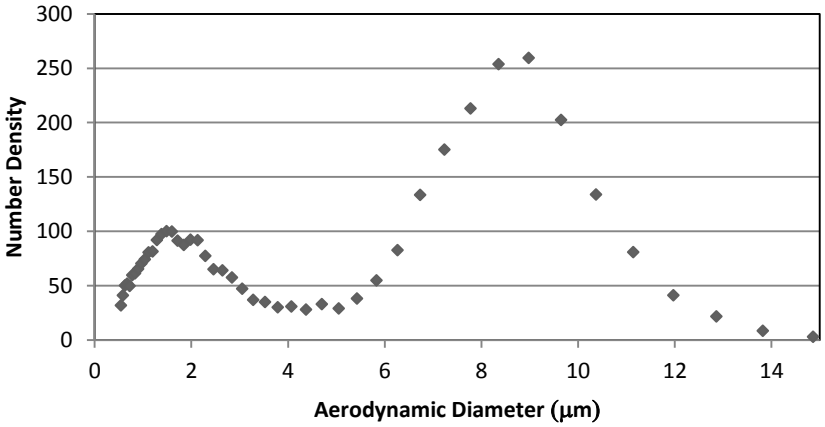

(c)

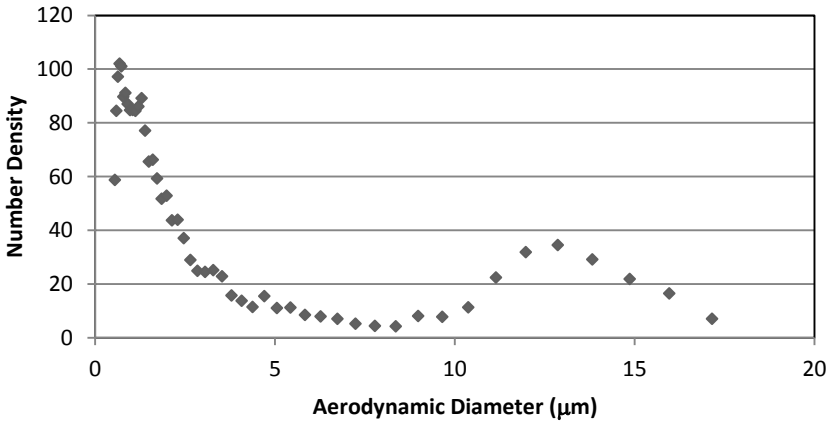

(d)

Figure 1. The particle distribution is measured in real time by an Aerodynamic Particle Sizer (APS). These figures show the distributions just after injection, when a maximum load of dust is lofted. Each of these trials used a 100 gram total dust loading for size cuts of: (a) 0-3, (b) 0-5, (c) 5-10, and (d) 10-20 microns.

2.2 Data analysis

Normalized transmission versus time curves are the ratios formed from dividing by the reference levels measured before each trial, for each of the visible and near infrared detectors. The long wave (LW) detectors require a digital lock-in amplifier to remove detector drift. The signal is corrected using a C-language program to take the raw data from the detectors at the laser chopper reference and smooth them using a running average of fifty data points for each transmission curve. Attention is given to the polarization of the lasers, the alignment of the polarizing beam splitting cubes at both ends of the chamber and also to possible contributions of reflection signals that could contaminate the measurements of polarization signals. Since the in-plane (in-polarization) signal is so much larger than the cross-polarization (depolarization) signal, we discover an influence in the cross-polarization channel of the in-plane signal. The depolarization value should not be quite zero in the absence of dust lofted in the chamber, since molecular scatter of the gas molecules in the air contribute to a background depolarization measurement [3]. We find a higher depolarization in the absence of aerosols than would be expected, suggesting the presence of in-plane polarization leakage. We correct both by subtracting a scaled output of the in-polarization detector, so that in the absence of aerosols in the chamber the depolarization has a zero value. For normalized data, the relation is

$$Depol_{Corr} = (Depol - (Depol_{Reference} / Trans_{Reference}) * Trans) * Gain_{Sys}, \quad (1)$$

where $Depol_{Corr}$ is the corrected depolarization, *Depol* is the normalized depolarization per time step, *Trans* is the normalized in-polarization measurement per time step, and $Gain_{Sys}$ is the ratio of the amplification of the detectors. The values with Reference subscripts are the quantities that the data are divided by for normalization, which causes the normalized data to have a unity value when no aerosols are present. Figure 2 demonstrates the correction for the forward depolarization. The curve describing the corrected ratio of the forward depolarization to the forward extinction is formed by subtracting the fraction of the forward transmission in-polarization measurement from the cross-polarization measurement.

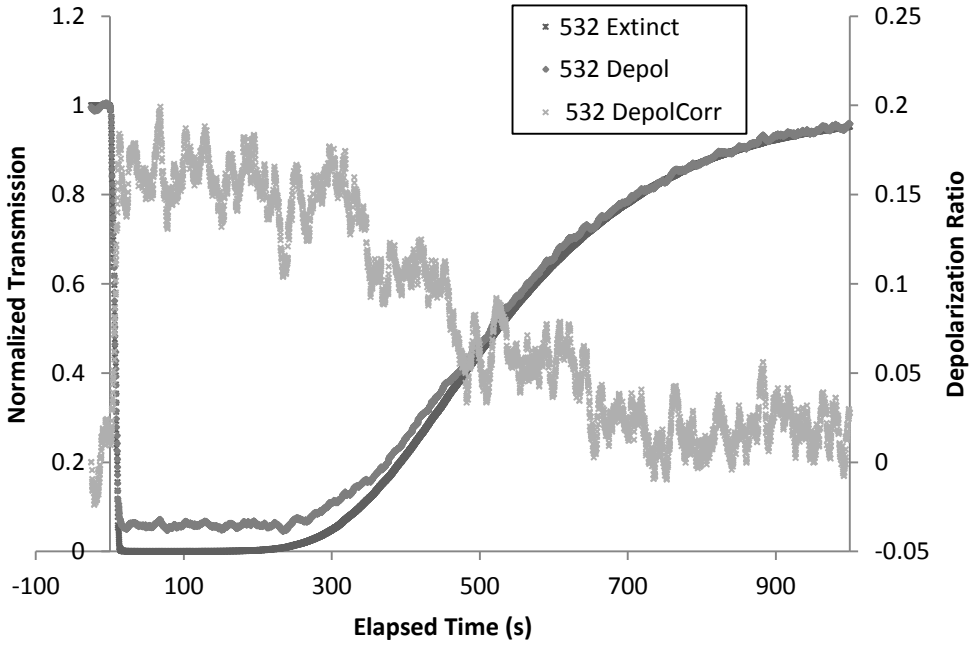

Figure 2. The values of the forward 532 nm in-polarization detector (532 Extinct) and the forward 532 nm cross-polarization detector (532Depol) are slightly different. The difference between the two values is the actual depolarization signal (532 DepolCorr). This case is for a 100 g loading with 0-3 μm ARD. The depolarization signal is zero before dust injection and returns to zero as the dust settles out. The magnitude peaks of the depolarization ratios are compared among the trials to determine wavelength, mass density and particle size dependencies.

3. RESULTS

This study addresses the primary issues of the origin of the depolarization signal, the generation of size-dependent extinction and depolarization values, and the testing of these values on data with overlapping size distributions. These topics are taken in order in the next few subsections. Evidence points to the lack of spherical symmetry as the cause for a depolarization signal for all cases but the maximum concentrations obtained at high loadings when multiple scatter is present. Size and wavelength dependent extinction scales with the particle size as expected for visible and near infrared wavelengths. The lack of absorption and the fact that the indices of refraction are similar at the visible and near-infrared wavelengths suggests that similar scattering will result, that only depends upon the cross section change with the particle size. The long wave data is different, the scattering cross-section values for large particles depart from the ν^4 (Rayleigh) dependence and both scattering and absorption are observed. At long wavelengths the absorption dominates for the small particles, because their scattering at LWIR is very small. Since the absorption efficiency is greater for small particles, when the absorption length is smaller than the particle size, it makes sense that the larger number of small particles can have a larger extinction than the larger particles, as is observed.

3.1 Evaluation of the depolarization signal

A depolarization signal can arise from either a lack of spherical symmetry or from multiple scattering processes. Our data includes enough different size distributions and wavelengths so that we can distinguish between the two causes. If the particles are not spheres, then they should always scatter to create some amount of depolarization. So the depolarization signal should always be a fixed fraction of the measured in-polarization signal for a particular size distribution of ARD. The scattered in-polarization signal is the departure of the normalized data from the 1.0 value. By contrast, multiple scattering depends nonlinearly on the number density at a higher power than one, because the value of the exponent depends upon the number of scattering events. Multiple scattering also produces a whitening of the scattering, meaning that all wavelengths have similar scattering extinction. This has been observed in lidar measurements of extinction through clouds, where UV and visible extinction values differ above and below the cloud where single scattering occurs, but become equal within the cloud, where multiple scattering dominates [4]. The dependence that we will most likely observe includes multiple scattering at higher densities. The key point is that there is a much stronger than linear dependence, so if the depolarization were due solely to multiple scattering, the depolarization signal would be expected to approach zero relatively fast as the number of particles settle out during a test.

In these trials the maximum value of the depolarization signal occurs at peak injection of the dust when the in-polarization signal is minimized. This signal can be used to separate the contributions of the particle shape from multiple scattering. Since we calculate the depolarization from normalized curves, the results are a normalized depolarization – it is normalized relative to the in-polarization data and it provides a very good approximation when the depolarization signal is small compared to the in-polarization signal. Examining the data from trials with different dust loading should show similar maximum values of the depolarization signal if the effect is due to non-spherical particles, while multiple scattering would favor significantly different values.

We obtain our first indication of the relative effects of spherical versus non-spherical particles in the depolarization measurements of the 10.6 μm beam, see Figure 3. The Ultrafine size cut which ranges from 0-15 μm has a peak in the particle distribution near 0-3 μm and a concentration level that represents a large optical depth in the beam that provides the only scattering. The form of the depolarization measurement follows the decay curve of the dust concentration levels in the chamber. The linearity can be checked by noting whether or not the two curves return half way to their final values at the same time, and by observing the tail of the process. All parts of the figure point to linearity, which is indicative of a non-spherical particle cause for the depolarization. The maximum value of the depolarization reached is 0.5 for both the 100 g and 200 g loadings of the Ultrafine size cut ARD, providing further evidence for this conclusion. The long saturation of the signal early in the 200 g loading trial is due to optical absorption at 10.6 μm.

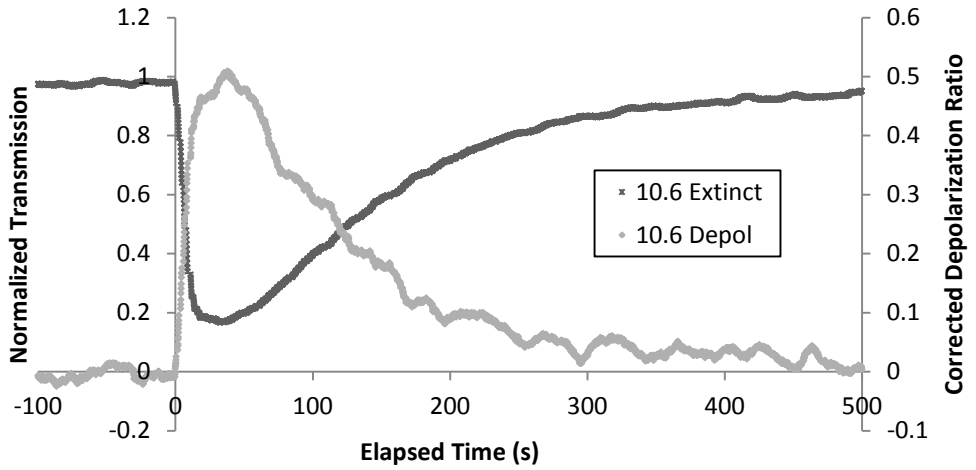

(a)

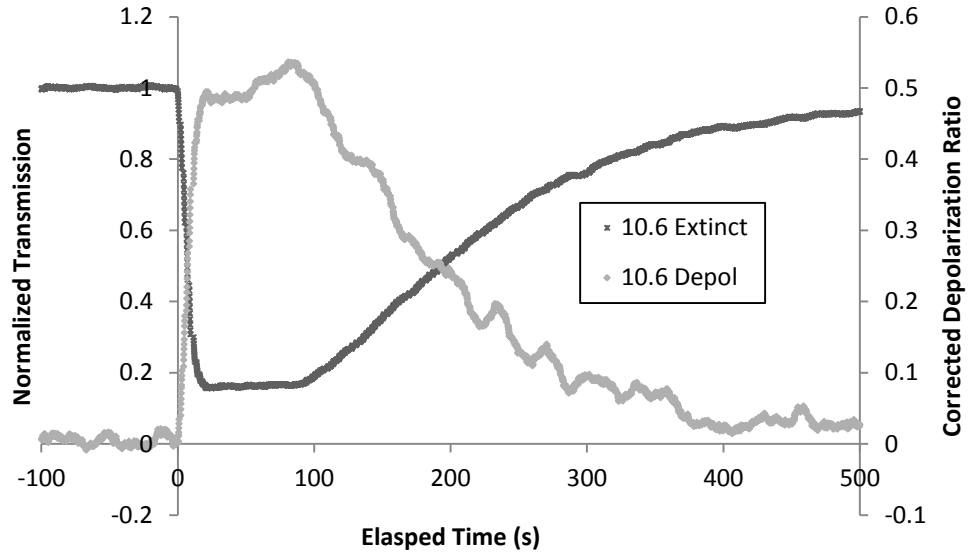

(b)

Figure 3. At an Ultrafine size cut of ARD, the 10.6 μm beam produces a depolarization signal that is not dependent on the concentration corresponding to loadings of (a) 100 g, and (b) 200 g. The normalized transmission value returns to unity with the settling of ARD out of the test chamber.

The data from the 532 nm beam show additional evidence for non-spherical particles in ARD. In Figure 2 and Figure 4 we compare depolarization measurements at a 100 gram loading in the four different size cuts. In Figure 2 we display a run at 0-3 μm. We see a peak in the depolarization at 0.17. Figure 4 displays runs of (a) 0-5 μm, (b) 5-10 μm, and (c) 10-20 μm. The 0-5 μm shows a peak at 0.03. The 5-10 μm shows a peak near 0.017. The 10-20 μm shows a peak at 0.0315. We see an inverse relationship with particle size for the smaller sizes. This is indicative of a particle shape property and not a population property. The increase in the peak for the largest particle size may be due to multiple scattering for this mass loading. We also learn from the seemingly uniform data of Figure 4 that the dusts of the different size cuts seem to be equally efficient at generating depolarized light. If, for example, the small dust was spherical and the larger dust eccentric, then the smaller dust would produce no depolarization while the larger dust would produce a significant amount. The uniformity suggests that the different sizes of dust are equally eccentric.

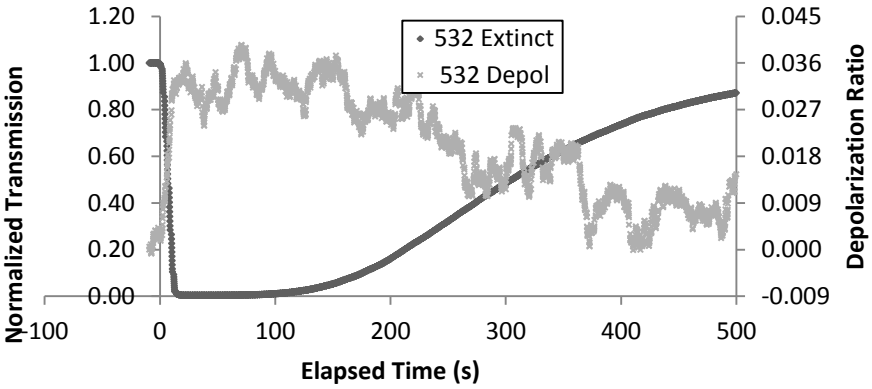

(a)

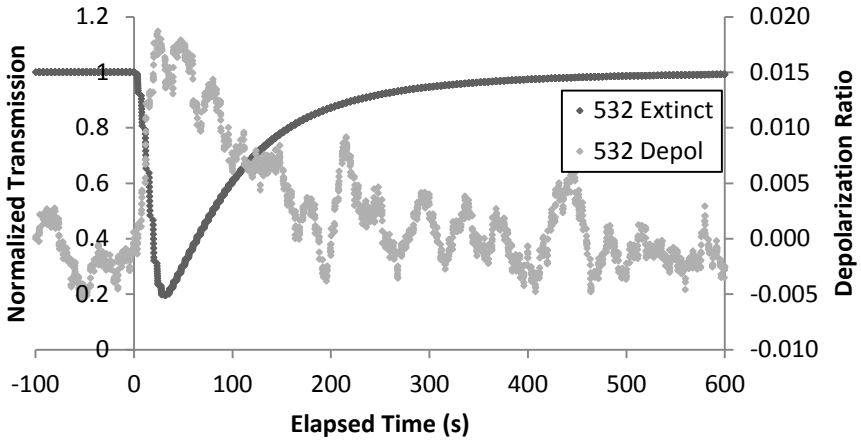

(b)

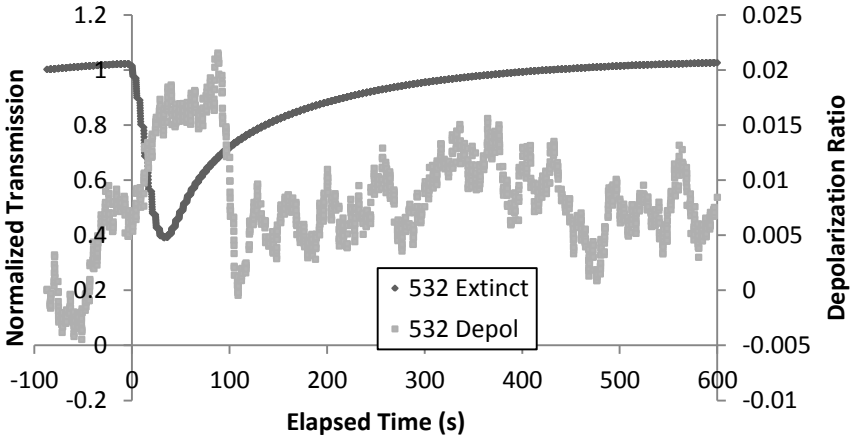

(c)

Figure 4. These three plots show the depolarization measurement for 532 nm at size cuts of (a) 0-5 μm, (b) 5-10 μm, and (c) 10-20 μm at a mass loading of 100 grams. Indications of non-spherical particles develop from the consistency of the depolarization curve for the changing conditions at smaller size cuts. In the largest size cut we see evidence for multiple scattering due to the mass density.

3.2 Qualitative aspects of the optical scattering

We first examine the forward extinction patterns that develop during various trials. Size cut selection has an effect, as does the concentration level in the aerosol cloud. The concentration of the particles determines the optical depth of the chamber for a particular test [2]. Larger particles have a short suspension time, even for a large chamber, considering the measurement for the 10 micron diameter particle size cut. The following plots, Figures 5-9, compare the transmission levels of three wavelengths for different concentration levels and size cuts of Arizona Road Dust. We list the size-cuts used in each test.

Figure 5 shows an example of the transmission measured at 0.532, 1.064, and 10.6 μm wavelengths for a particle size cut of 0-3 μm. This is a fairly light loading of the smallest size cut of dust. The size distribution does not cause a significant amount of the 10.6 μm beam to extinct. Even though this is the longest wavelength (10.6 μm) and smallest particles (0-3 μm), the median of the distribution is still large enough that the scattering is not quite in the Rayleigh regime, although it is fairly close to it, as indicated by the phase functions simulations in another paper of these proceedings [5]. The 532 nm and 1064 nm beams are in the Mie regime and are strongly scattered. The beam transmission is reduced to almost zero even with this light loading, but the number of particles is very large since we are loading by mass. Thus, the large extinction at the visible and NIR wavelengths is due to single scattering and multiple scattering by the particles. The transmission returns to unity as the particles settle out of the atmosphere of the test chamber. The settling time constant is quite long for small particles.

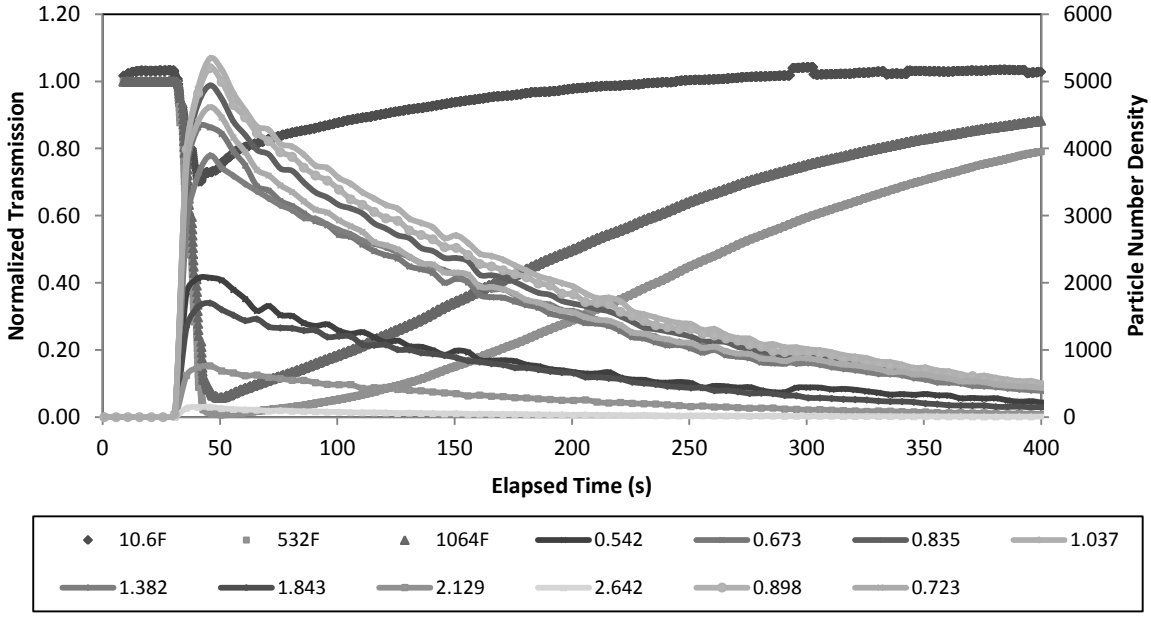

Figure 5. The optical transmission at several wavelengths (left axis) responds to scattering from 0-3 μm ARD particles as the size and number density (right axis) change as a function of time for a 20 g loading.

Figure 6 shows the measurements for a 0-5 μm sample of ARD at a concentration of 200 grams, which was the highest mass loading of dust for the series of tests. The higher loading and larger particles cause a much stronger response for the 10.6 μm beam than observed in Figure 5. The visible and near infrared beams show almost complete extinction (scattering of all wavelengths and absorption at LWIR) since the loading is heavy and the particles small, the number densities are very high. The small particles take a long time to settle out of the chamber, so this run is long, about 1.5 times longer than in Figure 5.

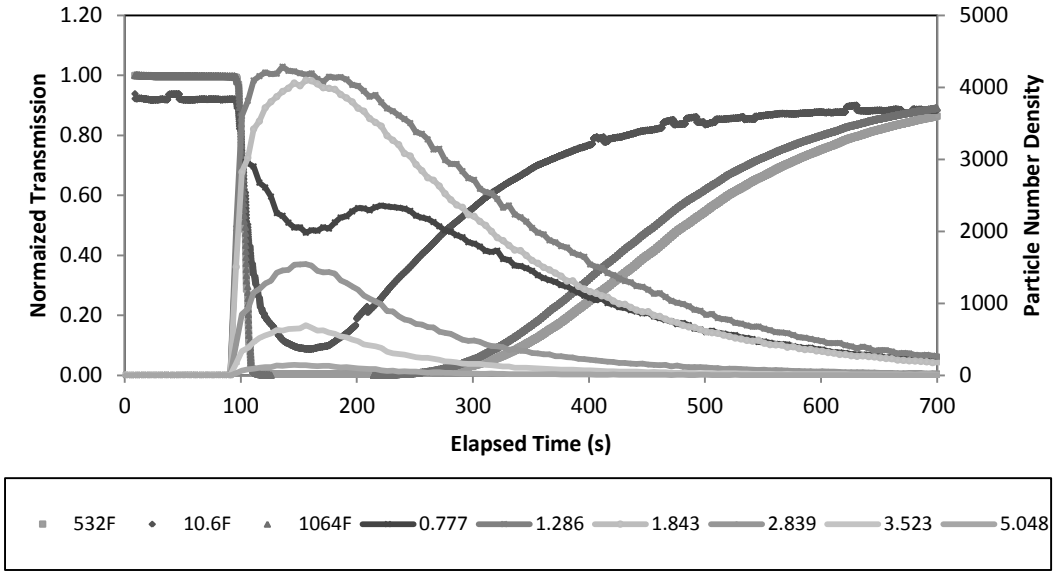

Figure 6. A loading of 200 g in the 0–5 μm size cut presents an optical thickness to all three beams that causes extinction over a longer interval. The density of the loading produces saturation in the 532 nm and the 1064 nm and exhibits the whitening characteristic of multiple scattering during injection.

Figures 7 and 8 show the same types of results as shown in Figures 5 and 6 for the size cuts 5-10 and 10-20 μm. These are larger particles, and the extinction in the long wave now contains scattering as well as significant absorption. The extinction in the long wave exceeds that in the visible and near infrared in both cases, at least at times not long after injection. This is due to the combination absorption at LWIR with multiple scattering for heavy loadings, as discussed above. The larger particles drop out of the distribution quite quickly, leaving only the smaller particles and reducing the component of multiple scattering. In fact, at later times during the run, the particle distribution begins to look more like the 0-5 micron distribution. Perhaps many of these particles are generated during the injection process by a break-up of a conglomerate or shed from the surface of a larger particle, but they settle out so slowly compared to the larger particles that they are still present at the end of a trial. Note the length of these runs is considerably shorter than for the smaller particles, even with the larger (100 or 200 gram) loadings, reflecting the faster dropout rate.

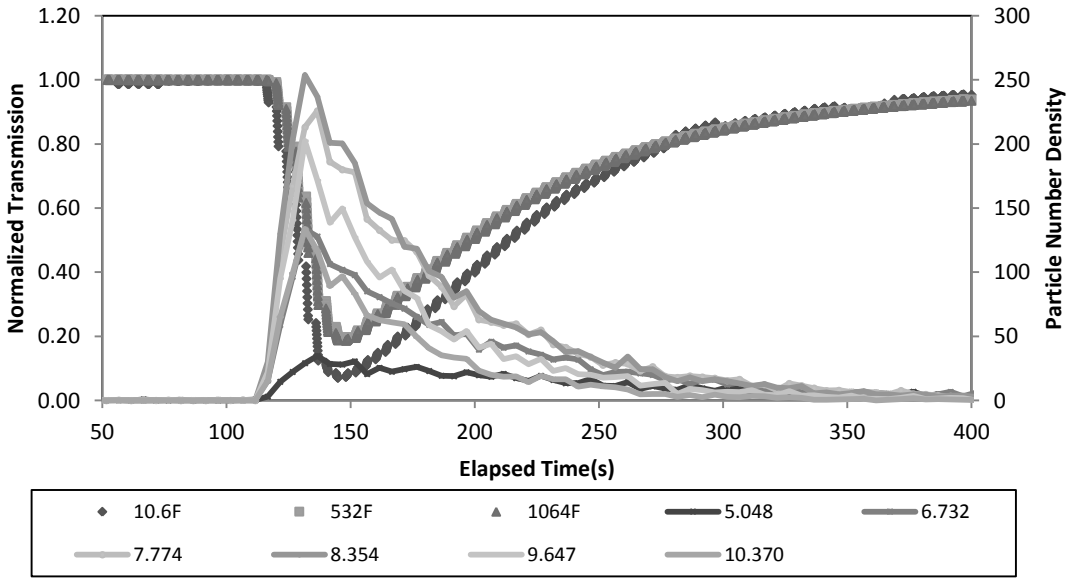

Figure 7. At the size cut of 5–10 μm, 100 g loading, the 10.6 μm beam undergoes significant scattering as well as absorption. The size of the particles ensures a short suspension time.

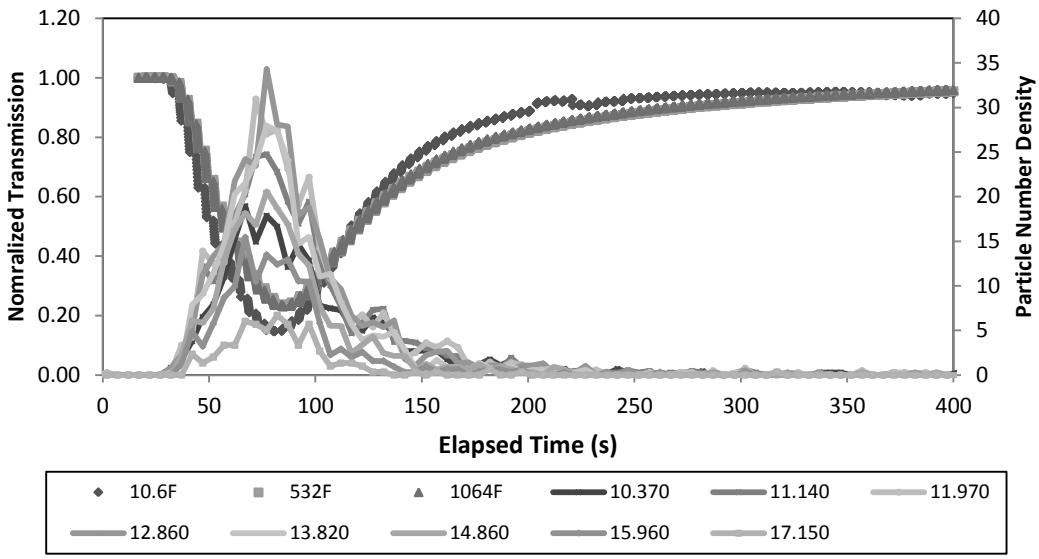

Figure 8. The size cut of 10-20 μm has the shortest suspension time; this has a 200 g loading. The different shape of this time sequence is caused by the process of injecting and the faster settling of these larger particles.

Figure 9 shows an example of optical measurements of a 0-10 μm particle size distribution. This size distribution causes the 10.6 μm to strongly scatter and absorb when there are large particles present in the distribution. As the larger particles rapidly settle out, the 10.6 μm signal recovers, while the visible and near infrared, 532 nm and 1064 nm signals, continue to be depressed by scattering from the smaller, longer-lived airborne particles. Wide particle distributions undergo the most dramatic changes during the settling process.

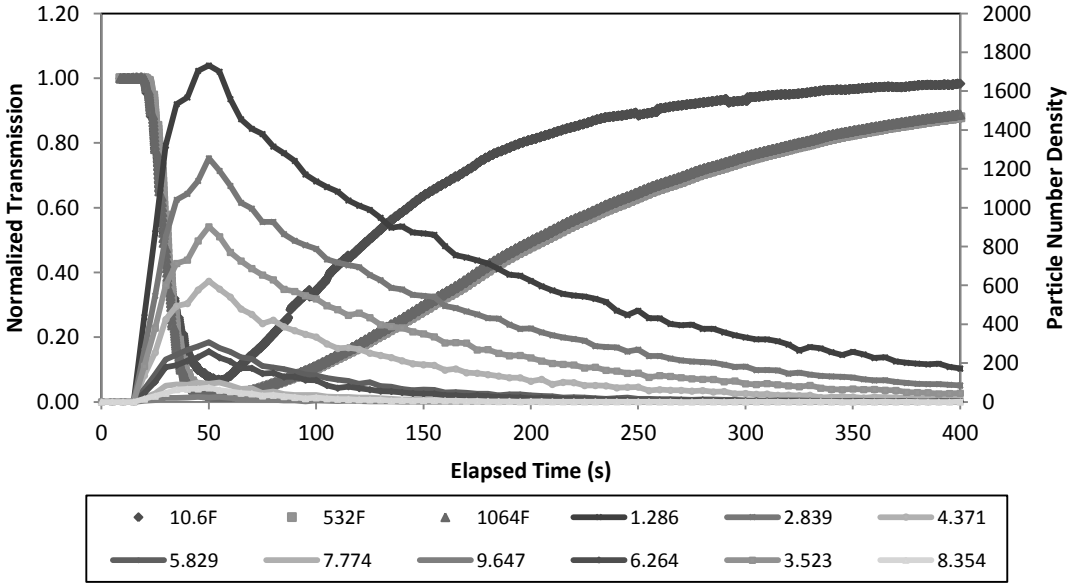

Figure 9. A sample with a particle size cut of 0-10 μm and 100 g loading causes the 10.6 μm wavelength to scatter much less when the only particles left are smaller than the wavelength.

3.3 Determination of the size-dependent extinction and depolarization

It is useful to be able to predict the extinction of an arbitrary size distribution. Since we have several size cuts that are almost non-overlapping, 0-5, 5-10, and 10-20 μm, see Figure 1, we can estimate the extinction of an arbitrary distribution by decomposing it into a sum of these three distributions. This would be mathematically sound if they were orthogonal and formed a basis, neither of which is true but both of which are approximately true. We take the number of particles in each distribution, and combine them as

$$I = I_0 \exp(-[N_1C_1 + N_2C_2 + N_3C_3]\, z), \quad (2)$$

where N_j are the number per volume for each distribution, I the extinction of optical irradiance for I_0 the input irradiance, z the length of the scattering volume, and C_j the extinction coefficients for each of our three size ranges that we calculate here [2].

The effective extinction coefficients, C, are determined using a simplified version of Equation 2 for which two of the N values are zero. These are the cases such as are shown in Figure 1. We note that even in these cases, there are some small particles present, so N_1 is never really zero. The numbers of small and desired particles are almost the same for the 10-20 μm trial and there will be more of the smaller particles than the desired ones later on. Since larger particles scatter more strongly than smaller ones, the smaller particles are assumed to be negligible at the peak density of the larger particles, just after injection. We can calculate C_1 first, and use it and Equation 2 to find the other C's, but do not. We obtain N by adding the number of particles per volume in the APS size bins corresponding to the mode of interest. A better estimate would assume that the extinction efficiency is approximately constant across the mode, so the cross sections within the mode depend only upon the particle area. Instead of simply counting the numbers in the size bins, we would scale the numbers by the squared size bin radius divided by the squared mode center radius before counting. In practice, these modes are symmetric and fairly narrow. Therefore the size effects are partially compensated and are not very large. We do not do this correction either. We know the path length, $z = 6.2$ *m*, from measurement. The quantity I/I_0 are the normalized values in curves of Figures 5-9 determine.

When we apply the method outlined above to all the time points of a trial, we obtain a value of C for each point along the curve, i.e., for each time step. Not all these C values are relevant. For example, the C values for times before injection should be zero since ideally $I/I_0 = 1$, but in practice, noise results in a deviation that is amplified by the small N at those times, causing a large noise fluctuation before injection. In trials with large particles such as mentioned above for the 10-20 μm size cut, just the first few time points after injection will be valid. Later, the smaller particles will begin to become more important, and we will be dividing by the wrong number (of the wrong size) of particles. These values of C will be wrong. The results look typically like those shown in Figure 10. The accurate value of C is that obtained when the particle concentration is still quite large. We use the values at the maximum aerosol density, and the corresponding data from the APS files. The units on C will be those of z divided by the volume used for the APS counts, and converted to μm^2. The results of the several runs are summarized in Table 1.

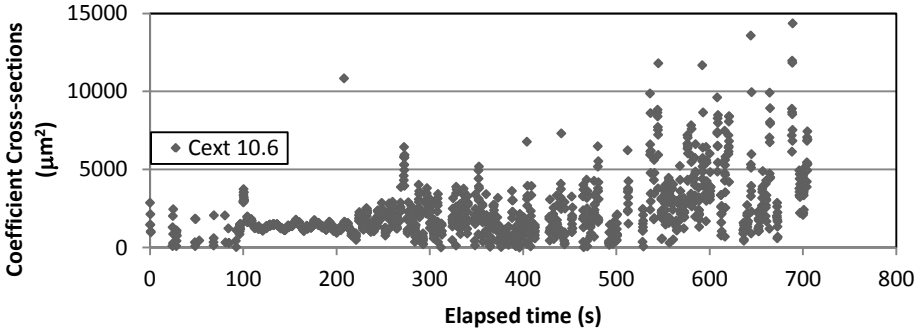

(a)

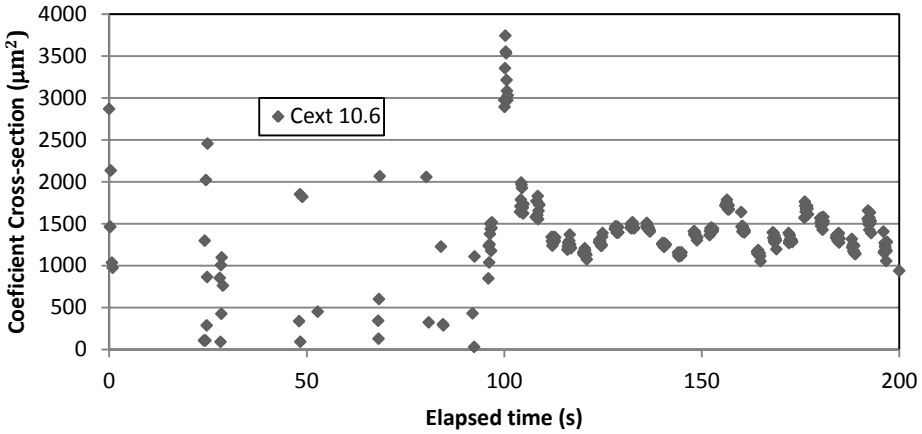

(b)

Figure 10. This example shows the determination of *C* from a time series of normalized intensities for a 100 g loading trial and the 10.6 μm wavelength. The data at the maximum number density, just after the injection period of the trial, produce valid *C* values. (a) The full range is in view, so the meaningless points with large noisy values are observed. Zooming in to the relevant region (b) shows the local minima with the actual value.

Table 1: The values of the effective per-particle extinction coefficient *C* in inverse square microns are calculated by inverting Equation 2 and selecting for the desired mode as a function of time.

Mode Size range, loading	532 nm	1064 nm	10.6 μm
0-3 μm, 100 g	10.093	6.432	1.223
5-10 μm, 100 g	158.66	164.11	272.10
10-20 μm, 100 g	790.49	846.35	1190

We test the utility of the coefficients of extinction from Table 1 by comparing measured extinction data to that calculated by breaking up the number distribution from the APS into 3 segments, counting particles, then predicting the extinction using Equation (2) and the values from Table 1. This process is repeated for many time steps during a trial. An example is shown in Figure 11, for a trial of 0-20 microns particles at 200 g loading. The results show reasonably good performance of the prediction method.

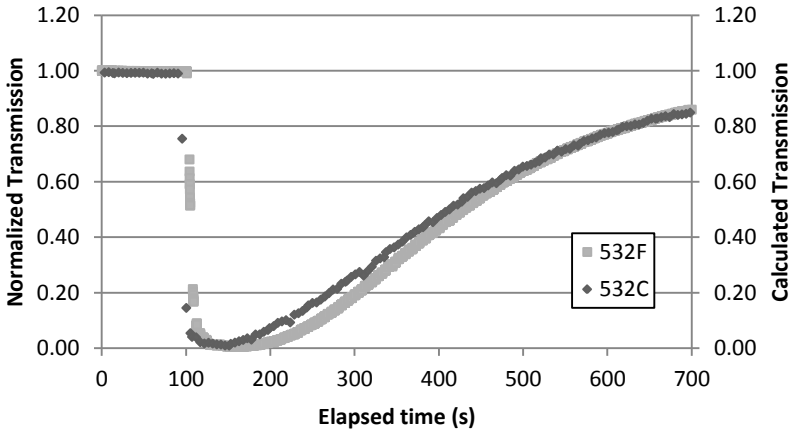

(a)

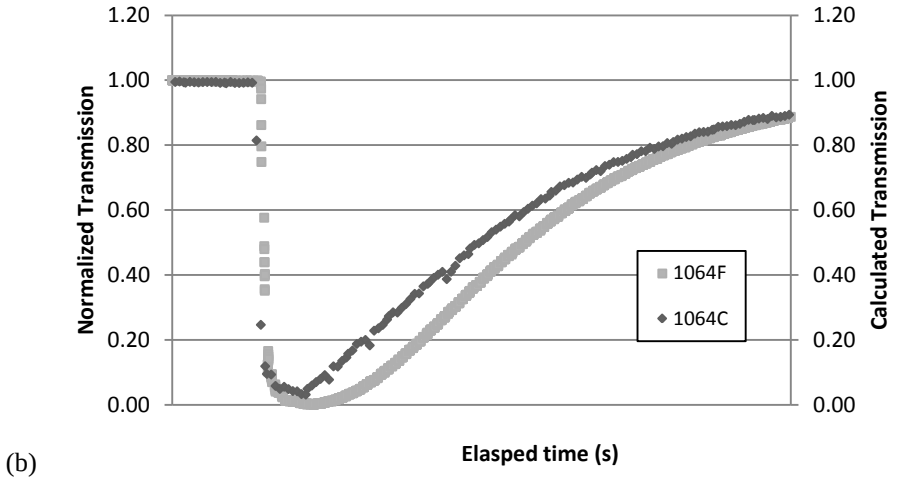

(b)

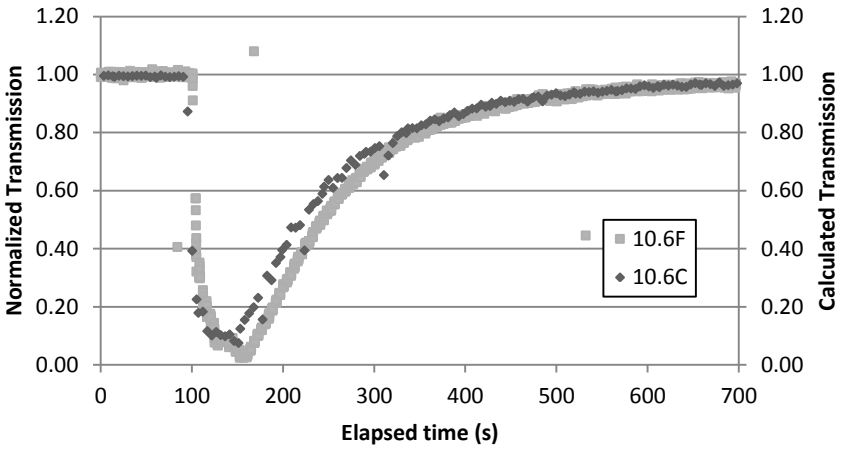

(c)

Figure 11. A comparison of a measured optical extinction for a broad distribution: 0-20 μm with the predicted extinction from a sum, Equation 2, of three modes (Figure 1), and scaled to approximate the actual size distribution as a function of time. We see close correlations between the measured optical extinction (designated F) and the predicted extinction (designated C) for: (a) 532 nm, (b) 1064 nm, and (c) 10.6 μm.

4. DISCUSSION

The qualitative aspects of extinction are observed for the wide range of size distributions studied. Small particles scatter the shorter wavelengths, the visible and near infrared, much more strongly than the long wave laser source. For larger particles, the long wave also scatters and its extinction is because both scatter and absorption are active at the long wave, while scattering is the important process for the shorter wavelengths studied. The larger particles settle faster, thus changing the size distribution as a function of time. The greatest change in the optical properties is observed when the initial distributions contain a wide range of particle sizes.

We find evidence of multiple scattering during the maximum number density of several heavy load trials, just after the injection process completes. This can be seen in Figures 7, and 8, which are data for both medium and large particles at high dust loading. Near the maximum density when the transmission is near minimum, the visible and near IR data lie on top of each other, illustrating whitening. The LWIR data exhibit a transmission lower than the visible and near IR at these times. This is due to a combination of whitening plus additional extinction from the absorption present at LWIR wavelengths but absent at the other wavelengths. In fact, when single scattering dominates and there is no whitening, the LWIR signals show less normalized transmission than the visible or near IR wavelengths. It is likely that multiple scattering is also observed at the visible and near-IR wavelengths near the maximum loading of the small particles in

Figure 6, just as it does in Figures 7-8. The LWIR does not show whitening (plus absorption) since it is scattered by these particles much more weakly than the shorter wavelengths. We do not detect multiple scattering for the trails with smaller loading or after a significant fraction of the particles have fallen out during any trial. Eccentric particles account for the most or all of the measured depolarization signals at lower densities. We have studied the eccentricity of the particles using microscopy and analyzed the effects of these eccentricities on exti
suggest that Mie calculations are valid for the optical extinction of particles found in ARD. The impact of these eccentricities, which have values less than 2 (few are greater than 1.5), is observed only at angles beyond the forward scattering lobe, and those are only strong for angles beyond the first secondary peak of the scattering phase function.

We have measured the effective per particle extinction coefficient for three reasonably narrow distributions, using the size cuts of ARD that are available commercially. They form a reasonable basis for understanding the optical properties of the set of all ARD size distributions. These results could be used to predict the extinction of an arbitrary ARD size distribution. An example is shown in Figure 11.

The cross section values determined for the modes deserve some comment. The scattering cross sections should approach twice the projected area of the particle as the particles get large compared to the wavelength, but approach zero for particles much smaller than the wavelength (near the Rayleigh limit) [1]. In the Mie scattering regime, with particle size comparable to the wavelength, the cross section can be larger or smaller than the projected area. We observe that the cross sections of the largest mode at the visible and near infrared wavelengths are similar in magnitude and approaching twice the projected area – the large particle limit. In contrast, the cross section of smallest mode for the LWIR light is much less than the projected area – nearing the Rayleigh limit. The other values in Table 1 are somewhat above the projected area of the mode, as expected for particles in the Mie regime.

5. CONCLUSION

The measurements at several wavelengths of a large number of size cuts and several loading masses (densities) of Arizona Road Dust allow a particle size-dependent comparison of optical scattering by ARD at several wavelengths. Qualitative features agree with expectations. Quantitative extinction cross sections hint at a size-dependent composition. A method of predicting extinction for an arbitrary ARD size distribution is presented. Depolarization patterns give evidence that ARD consists of non-spherical particles, with the eccentricity approximately independent of particle size. The results are beginning to answer the questions that affect the propagation of laser beams and the measurements by lidar in airborne particulate environments.

REFERENCES

[1] Bohren, C. F., Huffman, D. R., *Absorption and Scattering of Light by Small Particles*, Wiley-Interscience, New York, NY, (1998).
[2] Mischchenko, M.I, Travis, L. D., Lascis, A. A., *Scattering ,absorption, and emission of light by small particles*, Cambridge University Press, Cambridge, UK, (2002).
[3] Young, A. T., "Revised depolarization corrections for atmospheric extinction," Appl. Opt. 19, 3427-3428 (1980)
[4] Li, G. and Philbrick, C. R., "Lidar measurements of airborne particulate matter," Proc. of SPIE 4893, 94-104 (2002).
[5] Hallen, H. D., Hook, D. A., Pangle, G. E., Philbrick, C. R., "Multistatic Lidar Measurements of Non-spherical Particles," Under Review for SPIE Conference Paper 8731-25, (2013) (this proceedings).